Alexandria Engineering Journal (2013) 52, 717–731

Alexandria University

Alexandria Engineering Journal

www.elsevier.com/locate/aej
www.sciencedirect.com

ORIGINAL ARTICLE

Pressure integration technique for predicting wind-induced response in high-rise buildings

Aly Mousaad Aly *

Louisiana State University, Baton Rouge, LA, United States
Politecnico di Milano, Milan, italy

Received 2 July 2012; revised 18 July 2013; accepted 13 August 2013
Available online 26 September 2013

KEYWORDS

Dynamic response;
Finite element modeling;
Force balance measurements;
High-rise buildings;
Resilient structures;
Simultaneous pressure measurements;
Wind-induced loads;
Wind tunnel tests

Abstract This paper presents a procedure for response prediction in high-rise buildings under wind loads. The procedure is illustrated in an application example of a tall building exposed to both cross-wind and along-wind loads. The responses of the building in the lateral directions combined with torsion are estimated simultaneously. Results show good agreement with recent design standards; however, the proposed procedure has the advantages of accounting for complex mode shapes, non-uniform mass distribution, and interference effects from the surrounding. In addition, the technique allows for the contribution of higher modes. For accurate estimation of the acceleration response, it is important to consider not only the first two lateral vibrational modes, but also higher modes. Ignoring the contribution of higher modes may lead to underestimation of the acceleration response; on the other hand, it could result in overestimation of the displacement response. Furthermore, the procedure presented in this study can help decision makers, involved in a tall building design/retrofit to choose among innovative solutions like aerodynamic mitigation, structural member size adjustment, damping enhancement, and/or materials change, with an objective to improve the resiliency and the serviceability under extreme wind actions.

1. Introduction

1.1. Background

It is true that we cannot see the wind but we can see its effects. For instance, looking from a window and seeing branches and leaves of trees moving will give an indication that the weather is windy. Wind effects on the infrastructure can be low, moderate, strong, and extremely destructive. While low and moderate winds are beneficial for pollution dispersion and electric power generation, strong and extreme wind events can have devastating effects on the infrastructure. Extreme winds may

* Tel.: +1 (225)578 6654; fax: +1 (225)578 4945.
E-mail addresses: aly@LSU.edu, aly.mousaad@polimi.it.

Peer review under responsibility of Faculty of Engineering, Alexandria University.

Production and hosting by Elsevier

1110-0168 © 2013 Production and hosting by Elsevier B.V. on behalf of Faculty of Engineering, Alexandria University.
http://dx.doi.org/10.1016/j.aej.2013.08.006

cause damage to low-rise buildings in a form of windows damage, roof loss, or even complete collapse of wooden structures. In tall buildings however, both cladding loads and the dynamics of the structure become a concern. The use of high-strength, lightweight materials, longer floor spans, and more flexible framing systems results in structures that are more prone to vibrations. In tall buildings, wind events can cause severe and/or sustained vibratory motion, which can be detrimental to the structure and human occupants. Wind-induced vibrations may cause annoyance to the occupants (especially in the upper floors), impaired function of instruments, or structural damage. The evaluation of the wind-induced loads and responses is an important step for the design of the main force-resisting system of high-rise buildings, to balance safety and serviceability issues with the reality of limited resources.

1.2. Literature

Traditionally, wind-induced response of tall buildings in along-wind direction may be evaluated using formulae provided in the literature [15,14,11,21,1,9]. However, the literature has little guidance for the evaluation of the critical cross-wind and torsional responses. This is due to the fact that cross-wind and torsional responses result mainly from the aerodynamic pressure fluctuations in the separated shear layers and the wake flow fields, which made it difficult to have an acceptable direct analytical relation to the oncoming flow fluctuations [31,16]. In addition, the interference effects of surrounding tall buildings represent another challenge. Moreover, the responses evaluated using those formulae are restricted to a few modes, and the process depends on much assumption. On the other hand, wind tunnel pressure measurements and finite element (FE) modeling of the structures are the effective alternatives for determining these responses.

Wind tunnel tests have been industry wide accepted reliable tools for estimating wind loads on tall buildings. There are two types of rigid model testing that can provide overall structural wind loads. One technique relays on high-frequency base balance (HFBB) measurements and the other is based on high-frequency pressure integration (HFPI) of loads. Inherent in the HFFB approach is the fact that only the global wind loads at the base of the test model are known. The test results from the HFBB measurements can be analyzed using frequency domain or time domain techniques to get the building responses. The frequency domain approach has been dominant over time domain approach for its lesser requirement of computational power though it involves more approximations compared to the time domain approach. Nevertheless, with the current technology where computational power has been significantly improved, the time domain method will become a popular analysis technique. The time domain method allows the determination of wind responses directly from the equation of motion using the measured time history of wind loads, thereby avoiding all the simplifying assumptions used in the frequency domain method. However, even if the more accurate time domain approach is used for the analysis of the response, the three-dimensional (3D) mode shapes found in complex tall buildings complicate the use of the HFBB test results for predicting the structural response [24,13]. In general, mode shape correction factors for the HFBB technique are necessary for the assessment of wind-induced responses of a tall building. This is to account for the significant uncertainties in the estimation of generalized forces due to the nonideal mode shapes as well as presumed wind loading distributions [23,17]. HFPI technique with the time domain approach can be more accurate, providing that enough coverage of pressure taps on the model's outer surface is considered [22,3,5,2,19,30,31].

The HFPI technique is based on simultaneous pressure measurements at several locations on a building's outer surface. Pressure data can be used for the design of the claddings as well as the estimation of the overall design loads for the main force-resisting system. The HFPI technique cancels out any inertial effects that may be included in the overall loads measured by the base balance when the HFBB technique is used. Time histories of wind forces at several levels of tall building models can be obtained from a boundary-layer wind tunnel experiment, with a multichannel pressure scanning system. This enables the building responses to be computed directly in the time domain for buildings with simple or complex mode shapes.

Aly [2] used wind tunnel pressure data with a FE model of a tall building to predict its responses in the time domain. Yeo and Simiu [26] presented an illustration of the use of pressure time histories to estimate structural wind effects on tall buildings. The method allows for the estimation of the response from the time histories of simulated pressures at the exterior surface of a structure [27,25]. Yeo and Simiu [28] presented a procedure within a database assisted design (DAD) framework that accounts approximately for veering effects on tall building design. Their results show that veering effects on demand-to-capacity indexes for structural members are significant for certain building orientations, and that they increase with the length of the mean recurrence intervals.

1.3. Paper layout

The purpose of the study presented herein is to evaluate the responses of a high-rise building through the use of wind loads simulated in a boundary-layer wind tunnel and FE modeling of the full-scale structure. The study goes into the direction of comparing the results with recent design standards and the explanation of the physics behind the response of the building. The paper is organized as follows: In Section 2 a description of the boundary-layer test setup is presented. Section 3 introduces a modal approach to describe the dynamic behavior of a tall building under wind. Section 4 presents the HFPI approach followed to predict time histories of wind loads on a full-scale building. Section 5 presents the dynamic response of the tower obtained using the methodology followed in the current paper along with the comparison of recent codes and standards. Section 6 summarizes the conclusions drawn by the current study.

2. Experimental tests

The first step in the proposed procedure is to obtain time histories of actual wind loads on a tall building. This was achieved by a wind tunnel experiment on a high-rise building model which was carried out at the PoliMI wind tunnel, Milano, Italy [2,19]. The objectives of the tests were to conduct both pressure and force measurements on the building tower. Force measurements at the base of the model were conducted

using a six-component force balance. The pressure measurements were performed using high speed PSI-system 8400. The overall base loads obtained from the force balance measurements were compared with those attained from the integration of the pressures to ascertain enough pressure tap coverage.

The experiment was carried out in a boundary-layer test section of the wind tunnel of Politecnico di Milano (PoliMI). The dimensions of the test section are 4 m height, 14 m width and 36 m length. These huge dimensions allow for testing civil engineering structural models with large scales (up to 1:50) with low blockage effects. The long length of the test section allows for the turbulent boundary-layer to turbulence be fully developed. The empty test section provides a very uniform smooth flow. The boundary-layer thickness is about 0.2 m and the turbulence intensity I_u outside the boundary-layer is below 2%, due to a special type of painting used. Passive vortex generators in the form of spires, brick and roughness elements in the shape of pyramids were used at the entrance of the test section to simulate the growth of the boundary-layer. The configuration used represents a typical urban terrain profile [29]. Mean velocity profile normalized at a reference height of 1 m (which represents 100 m at full-scale) is shown in Fig. 1(a). It is worth noting that although the mean velocity profile can be obtained through simple measurements using a Pitot Static tube, a high sensitivity velocity measuring device is important to capture the flow fluctuations, and hence the turbulence intensities and the spectral content. Turbulence intensity profiles, integral length scale profiles, and the velocity spectrum at the reference height are shown in Fig. 1(b–d).

The building used in this study is 209 m × 57.6 m × 22 m steel tower with a total weight of 4×10^7 kg. A rigid model

Figure 2 Boundary-layer wind tunnel test setup of the tower and its surrounding. The surrounding structures within a radius of 500 m from the center of the tallest building were modeled on the turntable.

of the building was made of carbon fiber and scaled 1:100 (the tallest model in Fig. 2). To allow for pressure measurements, hundreds of pressure taps were instrumented on the outer surfaces through tubes passing through the outer skin of the model. These tubes were collected into groups (inside the test model) and then connected to individual pressure scanners. The measurements of the pressure distribution over the outer surface area of the model were conducted through a total number of 448 taps. The measurements of the pressure were carried out using a high speed PSI-system 8400; such system

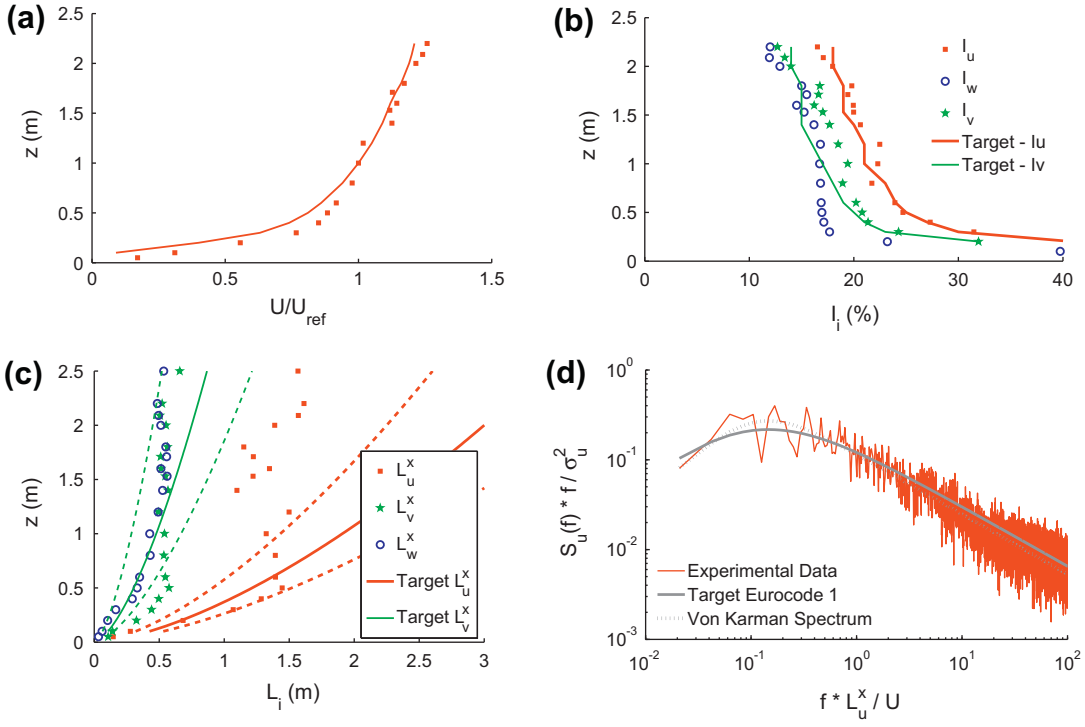

Figure 1 (a) Mean wind speed profile, (b) turbulence intensity profiles, (c) integral length scales, and (d) spectrum of the along-wind velocity component.

Figure 3 ESP pressure scanners with 16 and 32 channels. Due to their small size, they can be accommodated inside the test model (see [12]).

supports scanners of type ESP (see Fig. 3). Due to the small size of the scanner, it can be mounted inside the test model. This reduces the length of the pneumatic connectors used leading to an improvement in conducting measurements at high frequencies. Plastic tubes are used to connect the taps on the surface of the model to the scanners.

Overall wind loads at the base of the test model were measured using a stiff high-frequency balance. It is worth to mention that a high stiffness force balance was required to reduce the inertial effects under wind loads (rigid model experiment). The balance is capable of capturing six components of reactions at the base of the model (three components of force and three moments). Two accelerometers were mounted at the top of the rigid model from inside for acceleration measurements. These measurements were used later in order to remove the inertial effects from the force balance measurements to obtain the equivalent loads for the static case (in which the model is rigidly fixed with no flexibility).

The wind tunnel tests were conducted for 32 wind directions at 11.25° intervals for three different wind speeds. The pressure data were acquired at 22.5° intervals. The test was done for each one of the three buildings as alone and later for each building with the existence of the other models. Both force and pressure measurements were conducted over a time period of 2 min. Pressure and force data were acquired at sample rates of 62.5 Hz and 250 Hz, respectively.

3. FE modeling

The second step in the proposed procedure is to build the FE model of the full-scale structure to be used with wind load data in order to predict the dynamic behavior in a real world scenario. Fig. 4 shows the FE model of the full-scale building tower. The model has 2644 elements; each floor has a total number of 55 elements. Two main columns to carry the vertical loads were assumed to have hollow rectangular cross-sectional areas with a wall thickness varying with height in a step manner (rigidity changing with height). Floor masses were assumed to be distributed over the beams and the columns. The structural damping ratio for the first mode is 1%. The modal parameters of the FE model for the first six modes are given in Table 1. The equation of motion governing the behavior of the structure under wind loads is

$$M\ddot{X} + C\dot{X} + KX = F(t) \tag{1}$$

where M is a mass matrix, $X = [x, y]^T$ is a $2n \times 1$ vector and n is the number of nodes while x and y are vectors of displacements in x- and y-directions; C is a damping matrix and K is a stiffness matrix. $F(t) = [F_x(t), F_y(t)]^T$, in which $F_x(t)$ and $F_y(t)$ are $n \times 1$ vectors of external forces acting on the nodes in x- and y-directions, respectively. Using the first nine modes given from the FE model, with the next transformation

$$X = \Phi Q \tag{2}$$

In which **F** is $2n \times 9$ matrix of eigenvectors and Q is 9×1 vector of generalized displacements

$$\Phi = \begin{bmatrix} \phi_1(x_1) & \phi_2(x_2) & \dots & \phi_9(x_1) \\ \phi_1(x_2) & \phi_2(x_2) & \dots & \phi_9(x_2) \\ \vdots & \vdots & & \vdots \\ \phi_1(x_n) & \phi_2(x_n) & \dots & \phi_9(x_n) \\ \phi_1(y_1) & \phi_2(y_1) & \dots & \phi_9(y_1) \\ \phi_1(y_2) & \phi_2(y_2) & \dots & \phi_9(y_2) \\ \vdots & \vdots & & \vdots \\ \phi_1(y_n) & \phi_2(y_n) & \dots & \phi_9(y_n) \end{bmatrix}, \quad Q = \begin{Bmatrix} q_1 \\ q_2 \\ \vdots \\ \vdots \\ q_9 \end{Bmatrix}, \tag{3}$$

Substituting Eq. (2) into (1) and premultiplying by $\mathbf{F^T}$, one obtains

$$\Phi^T M \Phi \ddot{Q} + \Phi^T C \Phi \dot{Q} + \Phi^T K \Phi Q = \Phi^T F(t) \tag{4}$$

By assuming proportional damping, the above equation results in nine uncoupled equations

$$\left.\begin{aligned} m_{11}\ddot{q}_1 + c_{11}\dot{q}_1 + k_{11}q_2 &= \sum_{i=1}^{2n} \phi_1(x_i) F_{i,t} \\ m_{22}\ddot{q}_2 + c_{22}\dot{q}_2 + k_{22}q_2 &= \sum_{i=1}^{2n} \phi_2(x_i) F_{i,t} \\ m_{99}\ddot{q}_9 + c_{99}\dot{q}_9 + k_{99}q_9 &= \sum_{i=1}^{2n} \phi_9(x_i) F_{i,t} \end{aligned}\right\} \tag{5}$$

where m_{ii}, c_{ii}, and k_{ii} are generalized mass, generalized damping, and generalized stiffness of mode i, respectively. The $q_j(t)$ is then solved from each of the above equations. A MATLAB code was written to compute the time history of the responses [18].

4. Time history of the forces

The equations of motion defined in the previous section have the time history of the wind loads at full-scale as one parameter. So it is required to scale up the wind loads measured in the wind tunnel experiment. Using the measurements obtained by the pressure transducers, C_p at each tap was obtained as a function of both space and time. The geometric scale of the model to the prototype λ_L is 1:100. The mean wind speed at full-scale is assumed to be 30 m/s at a height of 100 m and the mean wind speed during the wind tunnel tests was 14.7 m/s. This gives a velocity scale λ_V of 1:2.04. Accordingly, the timescale can be calculated as $\lambda_T = \lambda_L/\lambda_V$ = 1:49. This

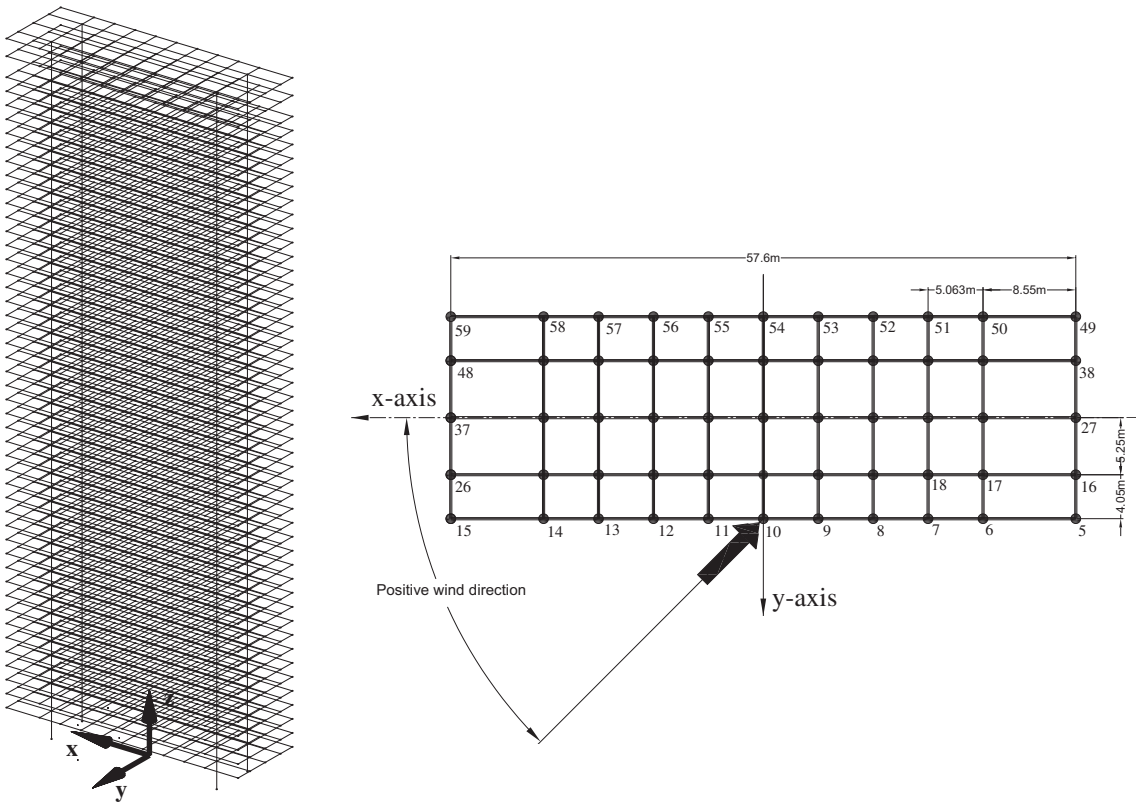

Figure 4 FE model of the full-scale building with the coordinate system and the wind direction reference.

Table 1 Modal parameters of the FE model.

Mode number	Generalized mass × 10e7 (kg m^2)	Generalized stiffness × 10e9 (N m)	Frequency (Hz)	Modal damping
1	1.2953	0.0147	0.1694	0.0102
2	0.9937	0.0178	0.2132	0.0112
3	0.4945	0.0222	0.3370	0.0150
4	0.8724	0.1115	0.5689	0.0234
5	0.8273	0.2153	0.8120	0.0326
6	0.3544	0.1600	1.0695	0.0426

Note: Modes 1 and 4 are lateral modes in x-direction; modes 2 and 5 are lateral modes in y-direction while modes 3 and 6 are torsional.

means that the 2 min wind data correspond to 98 min at full-scale. The pressure values on the surface of the full-scale model can be calculated as follows:

$$P(space, time) = \frac{1}{2}\rho V^2 C_p(space, time) \tag{6}$$

where $P(space, time)$ is a matrix containing pressure values on the surface of the full-scale model as a function of space and time, ρ is the air density which is assumed to be 1.225 kg/m^3, V is the mean velocity of the wind at full-scale, and C_p is the pressure coefficient obtained at the location of each tap as a function of time. The wind load at each node of the outer surface (see Fig. 5) is the integration of the pressure over the surface area in the vicinity of the node (tributary are, see [4]) as follows:

$$F(nodes, time) = \int P(space, time)dA. \tag{7}$$

This means that once the time history of the pressures on the outer surfaces is calculated, the external forces acting on the nodes of the surface can be computed. The excitation forces acting on the internal nodes are of course equal to zero. To allow for sufficient pressure measurements, 448 taps were mapped on the outer surface of the model (for the wind tunnel experiment). Pressure taps were distributed to cover the entire outer surface with more intense at the upper part of the test model (see Fig. 6(a)). Pressure data were integrated on the outer surface of the building (see Fig. 6(b)) to obtain the corresponding time history of wind loads. Codes were written in MATLAB to estimate the time histories of the wind forces acting at the center of each smaller area.

Mean wind loads along x- and y-direction as a function of the approaching wind direction are shown in Fig. 7. The wind loads measured by the balance are scaled up to represent the loads on the full-scale real building. It is shown that there is a good agreement between the results obtained by the balance and the pressure integration technique. It can be seen from the results presented in the figure that the effects from the surrounding tall buildings that have building heights about 71.8% and 81.3% of the tower height are significantly dependent on the incident wind direction. The effect is a reduction in the mean wind loads if the wind is coming from the direction of the surrounding buildings (sheltering effects). The maximum values of the mean wind loads in x- and y-direction occur at 202.5° and 270°, respectively. It can be seen also that magnitudes of the loads in the along-wind direction are larger than those in the cross-wind direction.

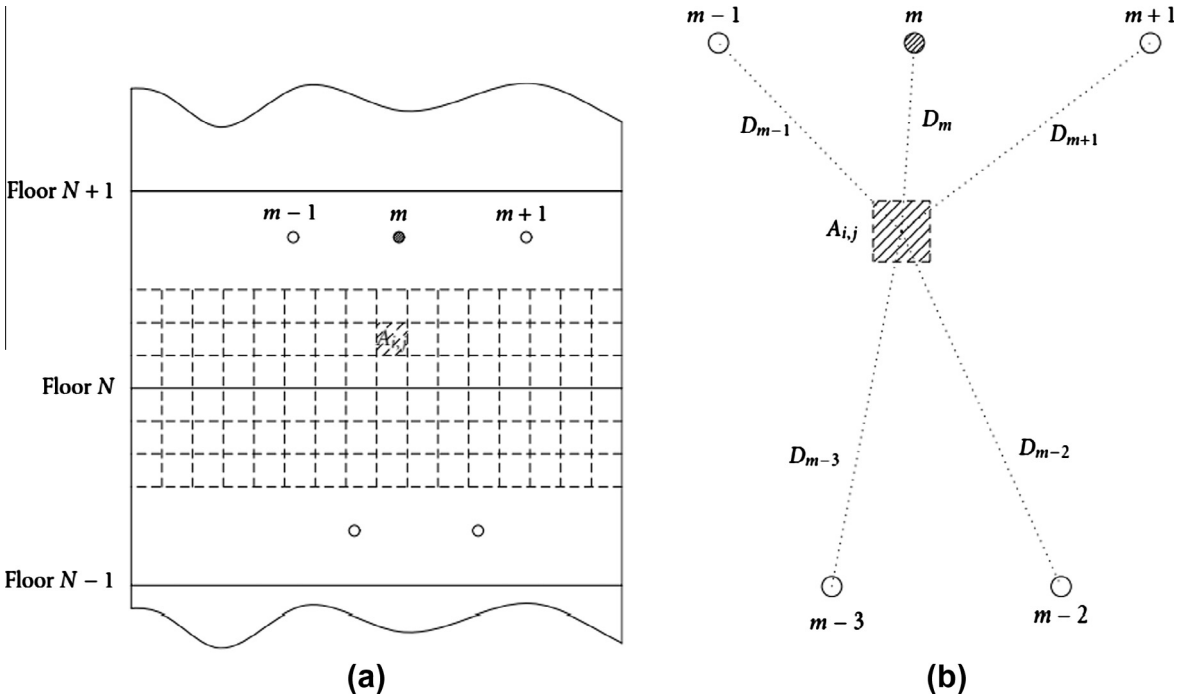

Figure 5 Wind load estimation from pressure data: the tributary area of floor N was divided into smaller areas; pressure forces acting on each smaller area A_i, were calculated based on pressure data at the nearest pressure tap, m.

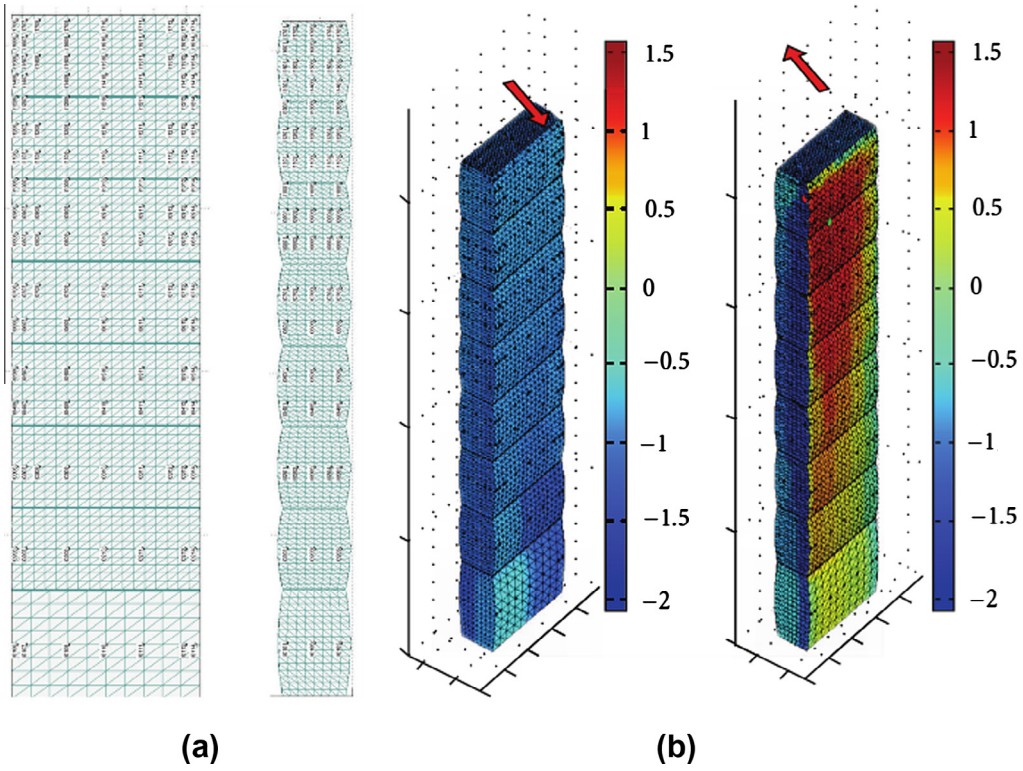

Figure 6 Pressures on the outer surface were obtained: (a) pressure tap distribution (elevation and side view), and (b) mean surface pressure coefficient distribution for a wind direction of 292.5°.

Fluctuating wind loads along x- and y-direction as a function of the approaching wind direction are shown in Fig. 8. The effect of the surrounding buildings is seen again as a dependent on the incident wind direction. The maximum values of the fluctuating wind loads in both x- and y-directions occur at an incident angle of 270°. The fluctuating wind loads

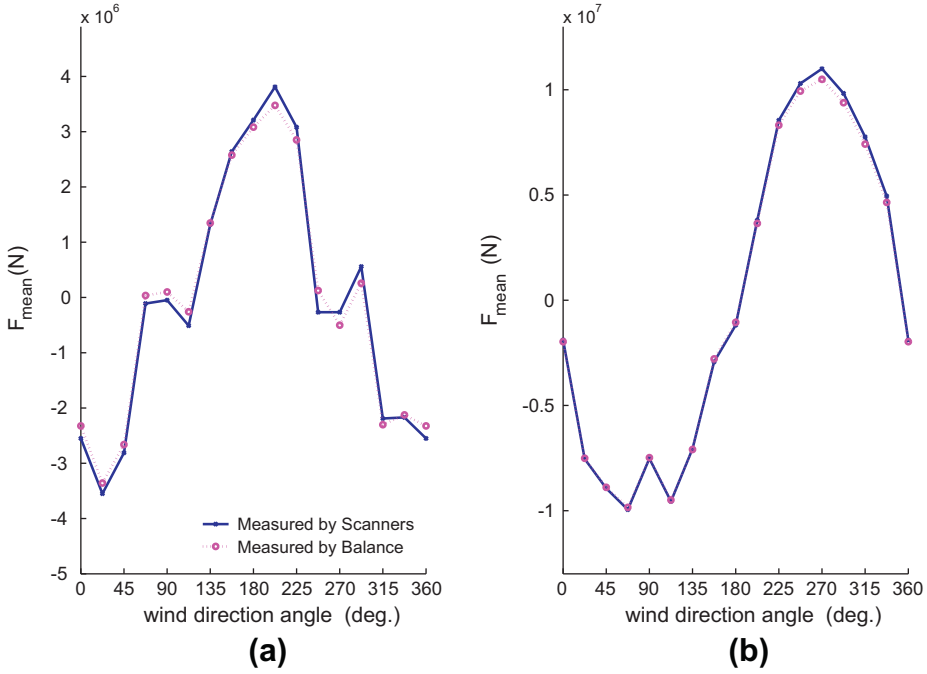

Figure 7 Mean wind loads as a function of the approaching wind direction: (a) x-direction and (b) y-direction.

in the y-direction are larger than those in the x-direction. This is due to the fact that the building is wider in the y-direction and thinner in the x-direction. However, the building is more flexible in the x-direction which means the dynamic displacements in this direction can be higher than that in the y-direction.

The generalized forces (GF) are obtained as follows:

$$GF = \Phi^T F(nodes, time). \tag{8}$$

Fig. 9 shows time history and Fast Fourier Transform (FFT) of the generalized forces for the first two modes under a wind direction angle of 270°.

5. Dynamic response

Table 2 gives the response of the tower in the along-wind direction and the cross-wind directions for a wind direction angle of

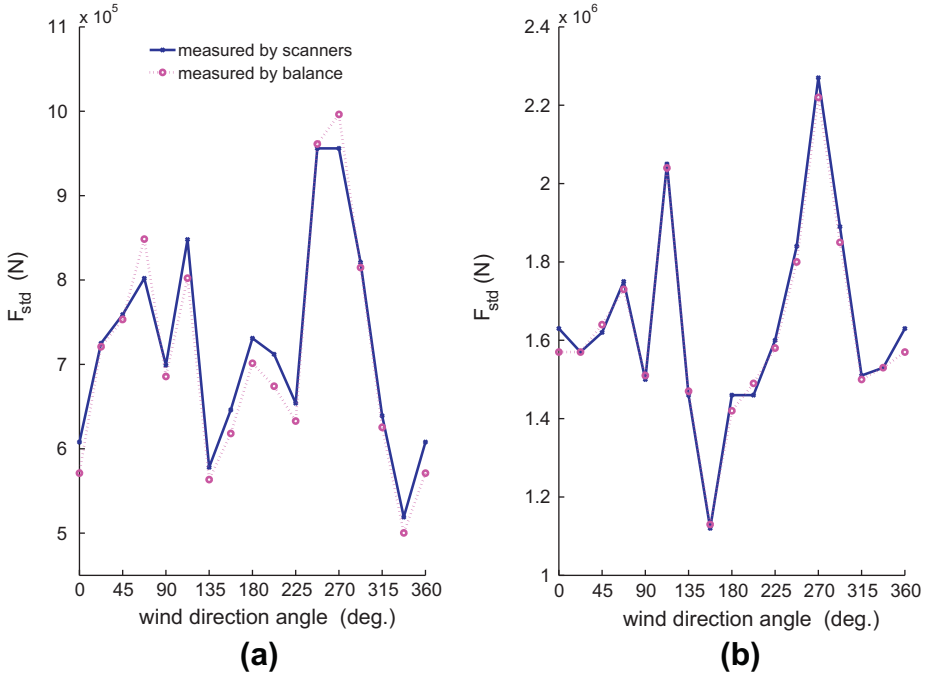

Figure 8 Standard division of the wind loads as a function of the approaching wind direction: (a) x-direction and (b) y-direction.

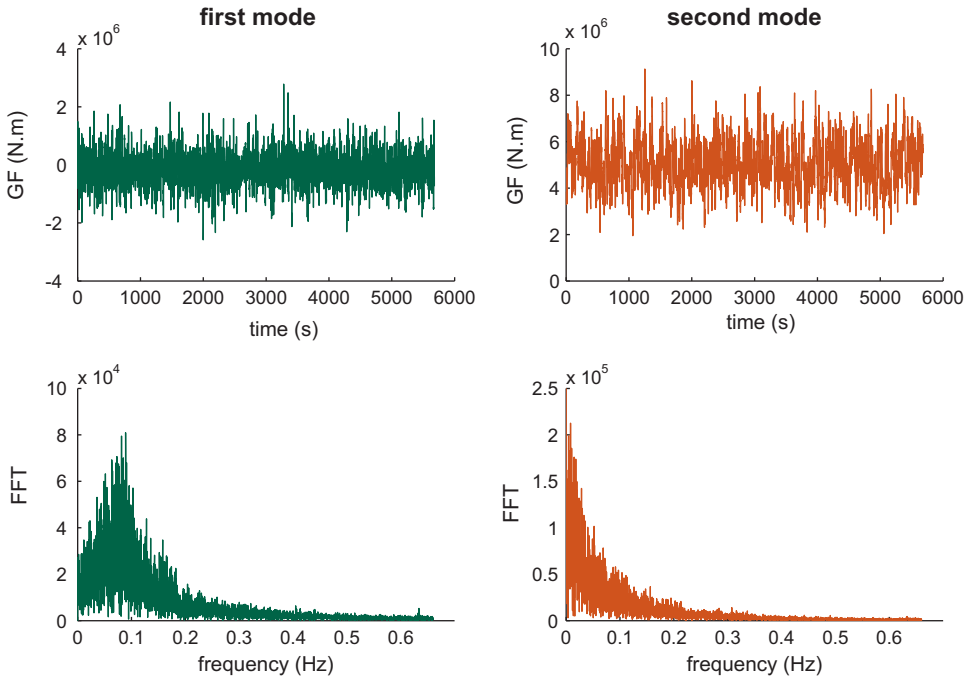

Figure 9 Generalized forces for an incident angle of 270°. *Note*: the mean value of loads is presented in the time history data (the second mode is mostly lateral vibration in the along-wind (y-direction)).

270° with different considerations of the mode shape. It is shown that the displacement response of the building may be evaluated by the first two vibrational modes. However, the acceleration response is contributed by not only the first two lateral vibrational modes but also by the contribution of higher modes. In any case, for accurate evaluation of the acceleration response it is important to consider not only the first two lateral vibrational modes but also higher modes. Ignoring contribution of higher modes may lead to underestimation of the acceleration response; however, it could result in overestimation of the displacement responses. After mode number 8 the change in the response is not significant. This is the reason for which only the first nine modes were considered. It is shown that the fluctuating cross-wind displacement (standard deviation) is higher than that of the along-wind.

Time history and FFT of the displacement and acceleration responses of the top corner of the building are shown in Figs. 10 and 11. Again it is shown that the acceleration response is contributed by higher modes of vibration while the displacement is dominant by lower modes.

Standard deviation (STD) of the displacements in x- and y-direction is shown in Fig. 12 as a function of the approaching wind direction. It can be seen from the figure that the maximum STD displacements of the building along x- and y-direction for all incident wind angles are 0.191 m and 0.135 m, which occur at 90° and 0°, respectively. Both directions are cross-wind for x- and y-direction, respectively.

Fig. 13 shows peak values of displacements of the top corner of the tower for both x- and y-direction as a function of the coming wind direction. The maximum displacements of the building along x- and y-direction for all incident wind angles are 0.704 m and 0.727 m, which occur at 292.5° and 270°, respectively.

STD acceleration responses of the top corner along x-axis and y-axis are shown in Fig. 14 as a function of the approaching wind direction. It is shown that the maximum STD

Table 2 Response of the top corner of the building tower for an incident angle of 270°.

Mode	σ_x, m		X_{mean}, m		$X_{\max}$, m		$\sigma_{\ddot{x}}$, m/s^2		$\ddot{X}_{\max}$, m/s^2	
	A	C	A	C	A	C	A	C	A	C
1	0.0003	0.1509	0.0000	0.0098	0.0013	0.5911	0.0004	0.1637	0.0014	0.6424
1:2	0.1177	0.1509	0.2818	0.0098	0.7510	0.5911	0.1805	0.1637	0.5616	0.6424
1:3	0.1188	0.1516	0.2770	0.0113	0.7350	0.5894	0.2018	0.1670	0.6904	0.6567
1:4	0.1188	0.1513	0.2770	0.0107	0.7350	0.5845	0.2018	0.1683	0.6904	0.6561
1:5	0.1182	0.1513	0.2696	0.0107	0.7243	0.5845	0.2037	0.1683	0.6693	0.6560
1:6	0.1183	0.1513	0.2701	0.0105	0.7257	0.5847	0.2071	0.1688	0.7079	0.6729
1:7	0.1183	0.1512	0.2701	0.0106	0.7257	0.5858	0.2071	0.1678	0.7079	0.7026
1:8	0.1183	0.1512	0.2708	0.0106	0.7270	0.5858	0.2078	0.1678	0.7315	0.7026
1:9	0.1183	0.1512	0.2708	0.0106	0.7270	0.5856	0.2078	0.1684	0.7316	0.7018

σ_x is the root mean square value of the fluctuating deflection, A means along-wind and C means cross-wind.

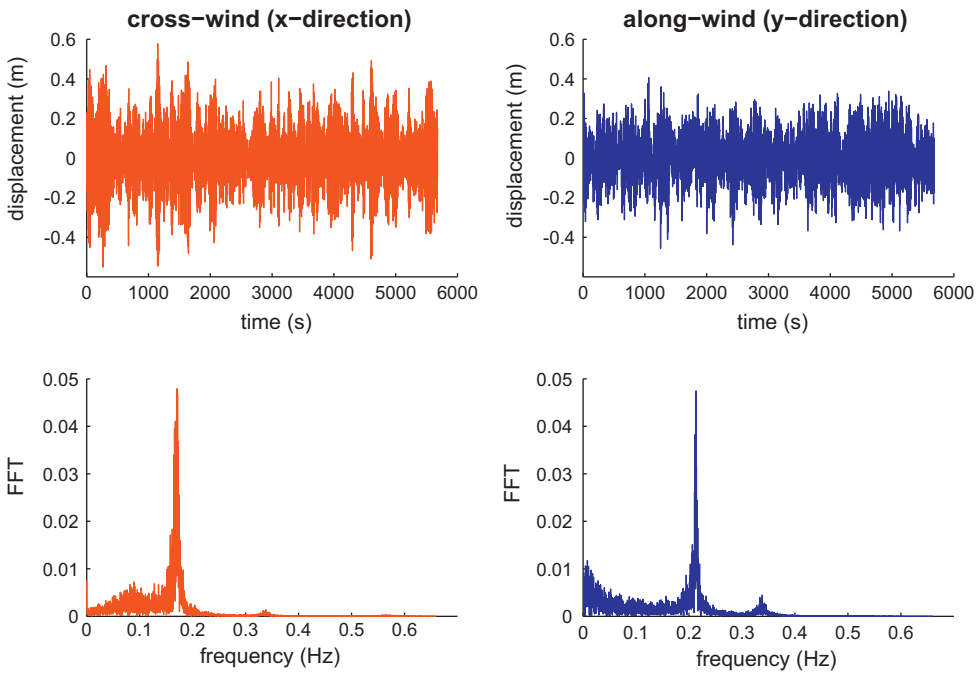

Figure 10 Top corner's displacement for a wind direction of 270°. *Note*: the mean value was subtracted from the time history data.

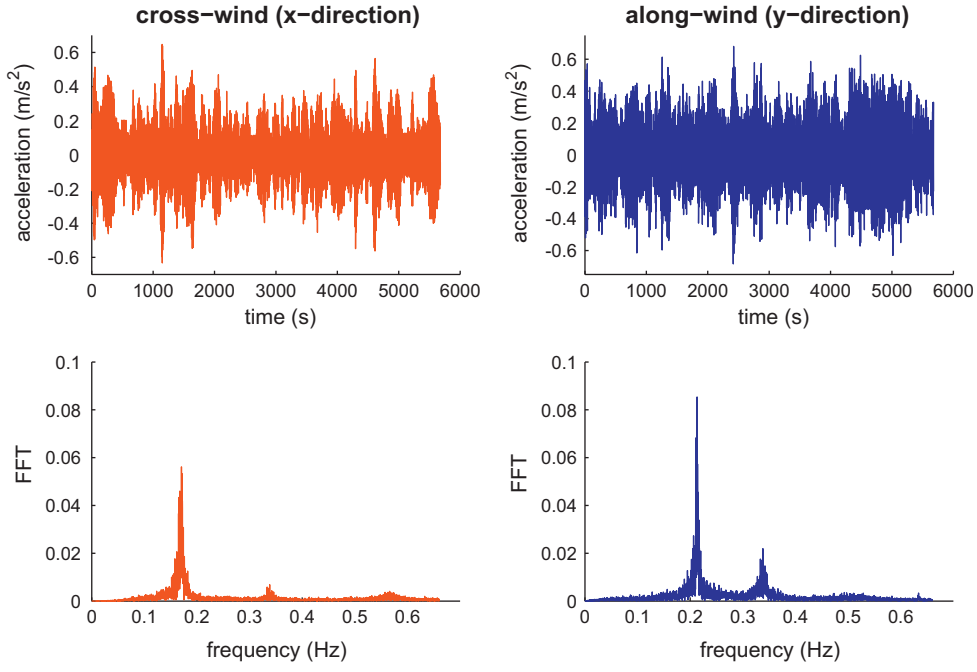

Figure 11 Top corner acceleration for a wind direction of 270°.

acceleration responses of the building along x- and y-direction for all incident wind directions are 0.222 m/s^2 and 0.273 m/s^2, which occur at 90° and 180°, respectively (cross-wind in both directions).

Maximum acceleration responses along x-axis and y-axis under the design wind speed action are shown in Fig. 15 as a function of the approaching wind direction. It can be seen from the figure that the maximum acceleration responses of the building along x- and y-direction for all incident wind angles are 0.847 m/s^2 and 1.122 m/s^2, which occur at 90° and 180°, respectively (cross-wind for both directions). Generally, the building acceleration is the most appropriate response component for checking the structural serviceability under wind loads. It is shown that the maximum acceleration is about 11.44% g which is considered by Simiu and Scanlan [20] to be *very annoying*. High responses are expected in this

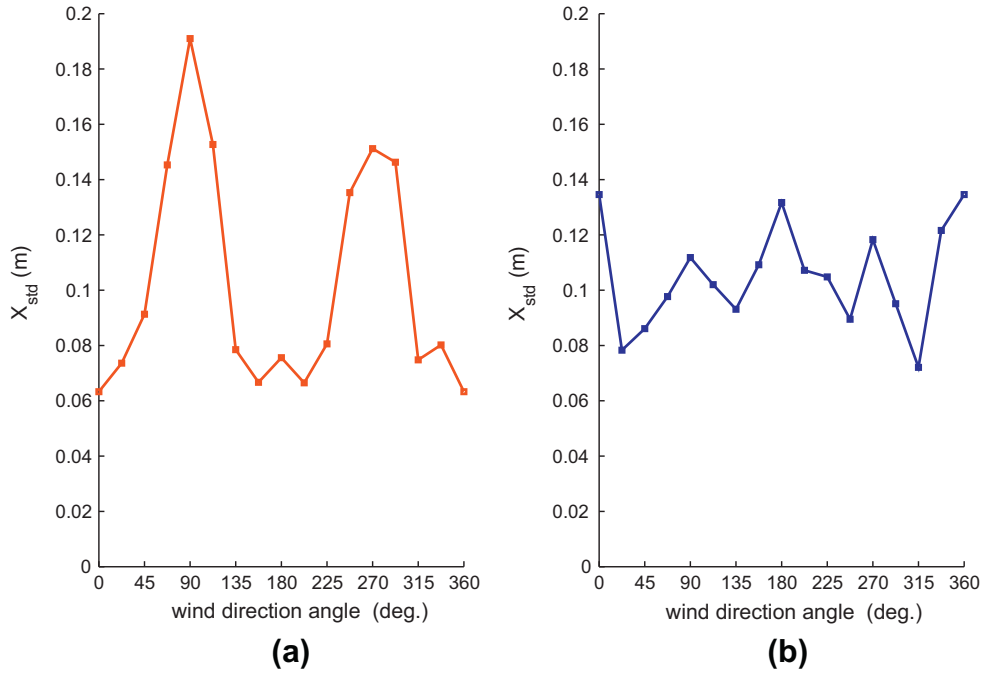

Figure 12 Standard deviation of the overall displacement of the top corner: (a) *x*-direction and (b) *y*-direction.

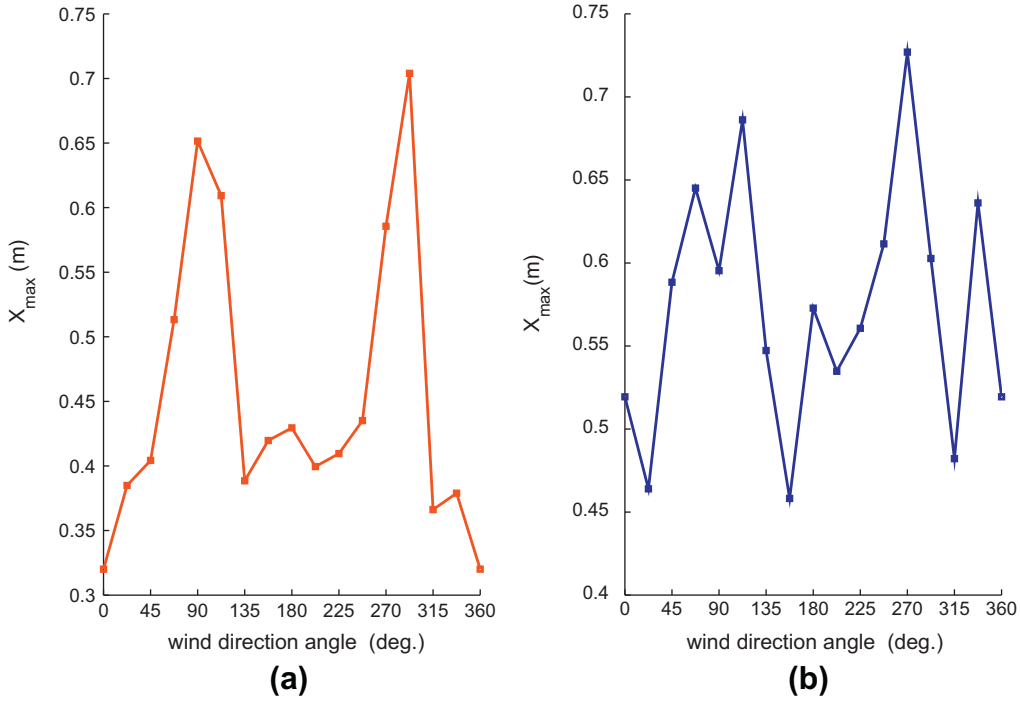

Figure 13 Peak values of the displacements of the top corner: (a) *x*-direction and (b) *y*-direction. *Note*: the mean value of displacements (due to static wind loads) was considered in the peak value analysis.

study because the wind profile used is highly turbulent and the structure is flexible with an aspect ratio of 9.5. In any case, a mitigation approach is presented in Aly et al. [3].

The Engineering Sciences Data Unit [10], the ASCE 7-2010 [1] and the Eurocode 1 [11] were used to obtain the along-wind response of the tower, assuming that the building shape is a rectangular prism. For the ASCE 7-2010, the basic wind speed is defined over a period of 3-*s*. Using the formula ([20], Eq. (2.3.37))

$$U_t(z) = U_{3600}(z)\left(1 + \frac{\beta^{1/2}c(t)}{2.5\ln(z/z_0)}\right) \tag{9}$$

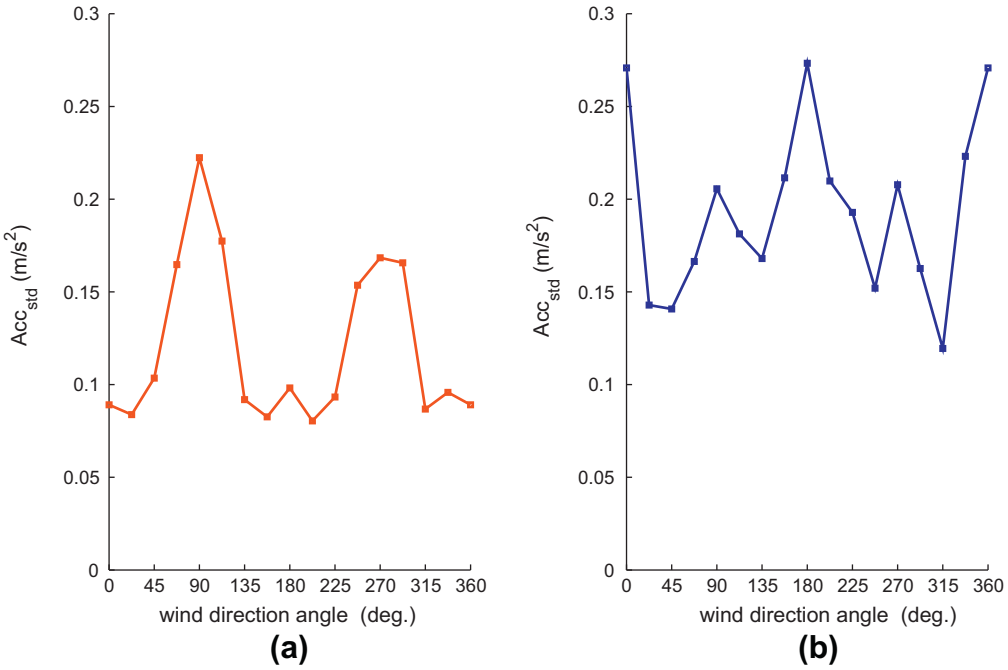

Figure 14 Standard deviation of the top corner accelerations: (a) x-direction and (b) y-direction.

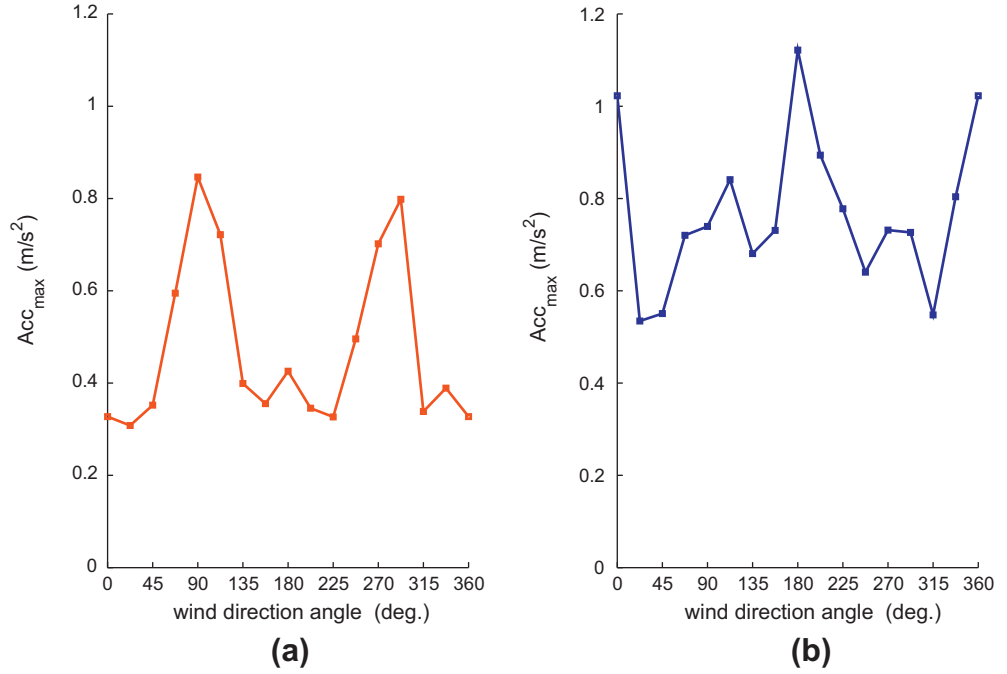

Figure 15 Peak accelerations of the top corner: (a) x-direction and (b) y-direction.

From Simiu and Scanlan [20] (Tables 2.3.1 and 2.3.3), $\beta = 5$ and $c(t) = c(600) = 0.36$ the mean hourly wind speed, $U_{3600}(10)$ is 22.3 m/s for $U_{3600}(10) = 25$ m/s. Again from the same equation for $c(t) = c(3) = 2.8$ the gust speed, $U_3(10)$ is 43.3 m/s.

Table 3 shows that there is a good agreement between the results obtained using the different codes and the results from the proposed method. Although the STD values of the acceleration obtained by the ASCE 7-2010 and the Eurocode are similar, the maximum values are different.

In conclusion, the methodology presented in the current paper has the advantages of considering complex shapes of structures with non-uniform mass distribution and can easily account for any required number of mode shapes to be considered in the response analysis. Wind-induced response analysis of tall buildings in their preliminary design stages can help

Table 3 Comparison of the along-wind responses obtained by the proposed procedure the response predicted by different design standards.

Results	ESDU	ASCE 7-2010	Eurocode 1	Proposed approach	
	90°	90°	90°	90°	270°
σ_x, m	0.102	–	0.1336	0.1118	0.1183
X_{max}, m	0.671	0.582	0.7114	0.5954	0.7270
$\sigma_{\ddot{x}}, m/s^2$	0.177	0.201	0.2083	0.2056	0.2078
$\ddot{X}_{max}, m/s^2$	0.785	0.764	0.6866	0.7395	0.7316

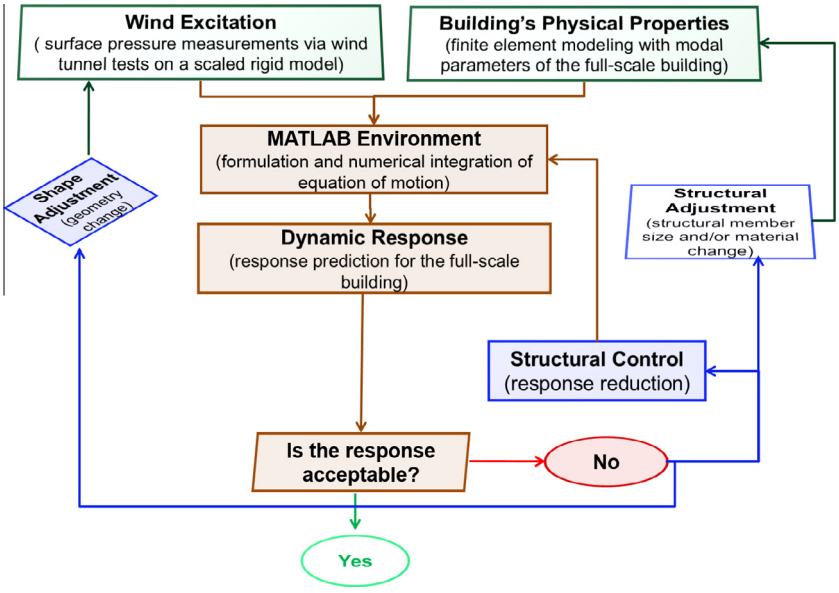

Figure 16 Schematic representation of a proposed decision making strategy, helpful in the design of high-rise buildings for wind.

decision makers to choose among potential mitigation solutions like aerodynamic shape modification, structural member size adjustment, and/or damping enhancement by passive, active, or semi-active control devices [3–8]. Fig. 16 shows a schematic representation of a proposed decision making strategy, helpful in the design of high-rise buildings for wind.

6. Concluding remarks

The paper presents practical procedure for response prediction in high-rise buildings under wind loads. To show the applicability of the procedure, aerodynamic loads acting on a quasi-rectangular high-rise building based on an experimental approach (surface pressure measurement) are used with a mathematical model of the structure for wind-induced response evaluation. The contributions of this paper can be summarized as follows:

- The case study building represents an engineered steel design of a structure that is very vulnerable to wind loads. This may be due to its low weight as well as high flexibility associated with the low dominant natural frequencies and the high aspect ratio.
- A good agreement in the predicted responses was found among the proposed approach and the most significant design standards (in the along-wind direction).
- The methodology based on HFPI and FE modeling, proposed for the estimation of the response of high-rise buildings under wind loads, has the advantage of combining lateral along-wind, lateral cross-wind, and torsional responses altogether. The proposed technique has the capabilities of considering structures with: (1) complex mode shapes, (2) non-uniform mass distribution, and (3) interference from the surrounding. In addition, the technique can account for the contribution of higher modes of vibration and the wind direction angle.
- The effect of the wind incident angle is very important as the maximum cross-wind response occurred at angle of 292.5° (at this angle it is difficult to calculate such response by traditional codes) rather than 90° or 270°. This is due to the interference effect caused by two tall buildings in the vicinity. However, this effect resulted into reduction in the mean wind loads and the associated maximum along-wind displacement, when the surrounding buildings were located in the upstream flow.
- The response of tall buildings in the cross-wind direction (lateral response combined simultaneously with torsion) can be higher than the response in the along-wind direction. This reveals the importance of the methodology presented in the current study, as the literature may provide accurate estimate of the along-wind response but less guidance for the estimation of the critical cross-wind and torsional response.

- For accurate estimation of the acceleration response it is important to consider not only the first two lateral vibrational modes but also higher modes. Ignoring contribution of higher modes may lead to underestimation of the acceleration response; however, it could result in overestimation of the displacement responses.

Acknowledgments

The author would like to express appreciation to the wind tunnel of Politecnico di Milano for the support he received during his stay in Italy. Many thanks to Professor Alberto Zasso and the Polimi's research team for their help.

Appendix A.

A.1. Calculation of the along-wind response using Eurocode 1

Note: All Expressions, Figures, Tables and Sections referred to in this appendix are the same as that stated in the Eurocode 1 [12].

The standard deviation of the turbulence σ_v may be determined using Expression (4.6).

$$\sigma_v = k_r \cdot v_b \cdot k_l$$

$$k_r = 0.19 \cdot \left(\frac{z_0}{z_{0,II}}\right)^{0.07}$$

z_0 is the roughness length, 0.7 m and $z_{0,II} = 0.05$ (terrain category II, Table 4.1) then $k_r = 0.2286$. $v_b = 25$ m/s, is the basic mean wind speed at a height of 10 m for a period of 10 min. k_l is the turbulence factor. The recommended value is $k_l = 1$. From the above expression $\sigma_v = 5.7138$ m/s.

The wind force F_w acting on a structure or a structural component may be determined directly by the Expression (5.3)

$$F_w = C_s C_d \cdot C_f \cdot q_q(z_e) \cdot A_{ref}$$

where $C_s C_d$ is the structural factor, C_f is the force coefficient for the structure or structural element, $q_q(z_e)$ is the peak velocity pressure (defined in 4.5) at reference height z_e, A_{ref} is the reference area of the structure or structural element.The structural factor $C_s C_d$ is given in Expression (6.1).

$$C_s C_d = \frac{1 + 2 \cdot k_p \cdot I_v(z_e) \cdot \sqrt{B^2 + R^2}}{1 + 7 \cdot I_v(z_e)}$$

in which $z_e = 0.6\,h = 125.4$ m and $I_v(z_e) = \frac{\sigma_v}{V_m(z_e)} = \frac{5.7138}{31} = 0.1843$. The turbulent length scale $L(z_e)$ represents the average gust size for natural winds. For heights z below 200 m the turbulent length scale may be calculated using Expression (B.1):

$$L(z) = L_t \cdot \left(\frac{z}{z_t}\right)^{\alpha}$$

with a reference height, z_t of 200 m, a reference length scale, L_t of 300 m, and with $\alpha = 0.67 + 0.05\ \ln(z_0)$. This gives $L(z_e) = 221.2616$ m.

The background factor B^2 allowing for the lack of full correlation of the pressure on the structure surface may be calculated using Expression (B.3):

$$B^2 = \frac{1}{1 + 0.9\left(\frac{b+h}{L(z_e)}\right)^{0.63}} = \frac{1}{1 + 0.9\left(\frac{57.6+209}{221.2616}\right)^{0.63}} = 0.4970$$

However, the value recommended by the code for B^2 is 1.

The resonance response factor R^2 allowing for turbulence in resonance with the considered vibration mode of the structure should be determined using Expression (B.6):

$$R^2 = \frac{\pi^2}{2\delta} S_L(z_e, n_{1,x}) R_h(\eta_h) R_b(\eta_b)$$

where δ is the total logarithmic decrement of damping given in F.5, S_L is the non-dimensional power spectral density function given in B.1 (2) and R_h and R_b are the aerodynamic admittance functions.

The logarithmic decrement of damping δ for fundamental bending mode may be estimated by Expression (F.15).

$$\delta = \delta_s + \delta_a + \delta_d$$

where δ_s is the logarithmic decrement of structural damping, δ_a is the logarithmic decrement of aerodynamic damping for the fundamental mode and δ_d is the logarithmic decrement of damping due to special devices (in this case δ_d is zero).

$$\delta_s = 2\pi\zeta = 2 \times 3.1416 \times 0.01 = 0.0628$$

The logarithmic decrement of aerodynamic damping δ_a for along-wind vibrations may be estimated by Expression (F.18).

$$\delta_a = \frac{C_f \rho V_m(z_e)}{2 n_1 \mu_e}$$

C_f is the force coefficient for wind action in the wind direction stated in Section 7 (see Eurocode 1). For a force blowing normal to a face

$$C_f = C_{f,0} \psi_r \psi_\lambda$$

where $C_{f,0}$ is the force coefficient of rectangular section with sharp corners, ψ_r is the reduction factor for square sections with rounded corners and ψ_λ is the end coefficient factor for elements.

From Fig. 7.23, $d/b = 0.3819$, $C_{f,0} = 2.25$. From Fig. 7.24 ψ_r is 1. From Fig. 7.36 considering $\varphi = 1$ and $\lambda = 70$ (from Table 7.16 consider case no. 4), $\psi_\lambda = 0.915$.

$$C_f = 2.25 \times 1 \times 0.915 = 2.0587$$

$$\delta_a = \frac{2.0587 \times 1.225 \times 31}{2 \times 0.21 \times (1.33 \times 10^7/(57.6 \times 209))} = 0.1681$$

$$\delta = 0.0628 + 0.1681 + 0 = 0.2309$$

The wind distribution over frequencies is expressed by the non-dimensional power spectral density function, $S_L(z,n)$ which should be determined using Expression (B.2)

$$S_L(z_e, n_{1,x}) = \frac{6.8 \times f_L(z_e, n_{1,x})}{(1 + 10.2 \times f_L(z_e, n_{1,x}))^{5/3}},$$

$$f_L(z_e, n_{1,x}) = \frac{n_{1,x} \times L(z_e)}{V_m(z_e)}$$

$$f_L(z_e, n_{1,x}) = \frac{0.21 \times 221.2616}{31} = 1.5$$

$$S_L(z_e, n_{1,x}) = \frac{6.8 \times 1.5}{(1 + 10.2 \times 1.5)^{5/3}} = 0.0974$$

The aerodynamic admittance functions R_h and R_b for a fundamental mode shape may be approximated using Expressions (B.7) and (B.8)

$$R_h = \frac{1}{\eta_h} - \frac{1}{2\times\eta_h^2}(1-e^{-2\eta_h}); \quad R_h = 1 \text{ for } \eta_h = 0$$

$$R_b = \frac{1}{\eta_b} - \frac{1}{2\times\eta_b^2}(1-e^{-2\eta_b}); \quad R_b = 1 \text{ for } \eta_b = 0$$

$$with: \quad \eta_h = \frac{4.6\times h}{L(z_e)} f_L(z_e, n_{1,x}) \text{ and } \eta_b = \frac{4.6\times b}{L(z_e)} f_L(z_e, n_{1,x})$$

$$\eta_h = \frac{4.6\times 209}{221.2616}\times 1.5 = 6.5127; \quad \eta_b = \frac{4.6\times 57.6}{221.2616}\times 1.5 = 1.7949$$

$$R_h = \frac{1}{6.513} - \frac{1}{2\times 6.513^2} = 0.1418; \quad R_b = \frac{1}{1.795} - \frac{1}{2\times 1.795^2} = 0.4019$$

then $R^2 = \frac{(3.1416)^2}{2\times 0.2309}\times 0.0974\times 0.1418\times 0.4019 = 0.1186$.

The peak factor k_p, defined as the ratio of the maximum value of the fluctuating part of the response to its standard deviation, should be obtained from Expression (B.4)

$$k_p = \sqrt{2\ln(vT)} + \frac{0.6}{\sqrt{2\ln(vT)}} \text{ or } k_p = 3 \text{ whichever is larger.}$$

The up-crossing frequency v should be obtained from Expression (B.5):

$$v = n_{1,x}\times\sqrt{\frac{R^2}{B^2+R^2}} = 0.21\times\sqrt{\frac{0.1186}{1+0.1186}} = 0.0684; \quad v > 0.08Hz$$

The limit of $v \geqslant 0.08$ Hz corresponds to a peak factor, k_p of 3. While T is the averaging time for the mean wind velocity, $T = 600$ s.

Referring back to Expression (6.1)

$$C_sC_d = \frac{1+2\times 3\times 0.1843\times\sqrt{1+0.1186}}{1+7\times 0.1843} = 0.9473$$

From Expression (5.3)

$$F_w = 1.9504\times q_q(z_e)\times A_{ref} = 1.9504\times\left(\frac{1}{2}\rho\times V_m^2(z_e)\right)\times(b\times h)$$

To determine the peak response of the tower, the peak velocity pressure q_p at height z_e should be considered instead of q_q in the above equation. The recommended rule to determine q_p is given in Expression (4.8).

$$q_p = [1+7\times I_v(z_e)]\times\frac{1}{2}\times\rho\times V_m^2(z_e)$$

that gives $F_{w,\max} = 4.4667\times(\frac{1}{2}\rho\times V_m^2(z_e))\times(b\times h)$.

The mean displacement, X_{mean} and the maximum displacement, $X_{\max}$ are determined using F_w and $F_{w,\max}$ respectively. The root mean square value of the fluctuating deflection, σ_x is determined using the definition of the peak factor, k_p [21]

$$\sigma_x = \frac{X_{\max} - X_{mean}}{k_p}$$

The standard deviation $\sigma_{a,x}$ of the characteristic along-wind acceleration of the structural point at height z should be obtained using Expression (B.10)

$$\sigma_{a,z}(z) = \frac{C_f\rho b I_v(z_e)V_m^2(z_e)}{m_{1,x}} RK_x\Phi_{1,x}(z)$$

K_x is the non-dimensional coefficient, given by Expression (B.12)c

$$K_x = \frac{(2\zeta+1)\left\{(\zeta+1)\left[\ln\left(\frac{z_e}{z_0}\right)+0.5\right]-1\right\}}{(\zeta+1)^2\ln\left(\frac{z_e}{z_0}\right)}$$

$$\sigma_{a,z}(z) = \frac{2.0587\times 1.225\times 57.6\times 0.1843\times 31^2}{(1.33\times 10^7/209)} \times 0.3444\times 1.5\times 1 = 0.2083 \text{ m/s}^2$$

Using Expression (B.4) and replacing v by n_1; the peak factor for the acceleration is 3.2957 which gives a maximum along-wind acceleration of 0.6866 m/s^2.

References

[1] ASCE 7-2010, Minimum Design Loads for Buildings and Other Structures, ASCE Standard, ASCE/SEI 7-10, American Society of Civil Engineers, Reston, Virginia, 2010.

[2] A.M. Aly, On the Dynamics of Buildings Under Winds and Earthquakes: Response Prediction and Reduction. Ph.D. Dissertation. Department of Mechanical Engineering, Politecnico di Milano, Milan, Italy, 2009.

[3] A.M. Aly, F. Resta, A. Zasso, Active Control in a High-rise Building Under Multidirectional Wind Loads. SEI 2008 Structures Congress – Vancouver, Canada, April 24–26, 2008, doi: 10.1061/41016(314)285.

[4] A.M. Aly, Proposed approach for determination of tributary areas for scattered pressure taps, Wind and Structures 16 (6) (2013) 617–627.

[5] A.M. Aly, A. Zasso, F. Resta, Dynamics and control of high-rise buildings under multidirectional wind loads, Smart Materials Research 2011 (2011) 549621, http://dx.doi.org/10.1155/2011/549621 (15pp).

[6] A.M. Aly, A. Zasso, F. Resta, On the dynamics of a very slender building under winds: response reduction using MR dampers with lever mechanism, The Structural Design of Tall and Special Buildings 20 (5) (2011) 541–553, http://dx.doi.org/10.1002/tal.647.

[7] A.M. Aly, Proposed robust tuned mass damper for response mitigation in buildings exposed to multidirectional wind, The Structural Design of Tall and Special Buildings (2012), http://dx.doi.org/10.1002/tal.1068.

[8] A.M. Aly, Vibration control of high-rise buildings for wind: a robust passive and active tuned mass damper, Journal of Smart Structures and Systems (2013) (in press).

[9] S.X. Chen, A more precise computation of along wind dynamic response analysis for tall buildings built in urban areas, Engineering 2 (2010) 290–298.

[10] Engineering Sciences Data Unit, Response of Structures to Atmospheric Turbulence: Computer Programs A9236 and B9236. ESDU Item 92036, Aerospace & High Technology Database (CSA), London, UK, 1992.

[11] Eurocode 1, Actions on Structures – Part 1-4: General Actions – Wind actions. prEN 1991-1-4, European Standard, 2004.

[12] ESP, ESP Pressure Scanner: User's Manual, Pressure Systems, Inc., Hampton, VA, USA, 2009.

[13] M.F. Huang, K.T. Tse, C.M. Chan, et al, An integrated design technique of advanced linear-mode-shape method and serviceability drift optimization for tall buildings with lateral-torsional modes, Engineering Structures 32 (8) (2010) 2146–2156.
[14] A. Kareem, Dynamic response of high-rise buildings to stochastic wind loads, Journal of Wind Engineering and Industrial Aerodynamics 42 (1–3) (1992) 1101–1112.
[15] A. Kareem, Aerodynamic response of structures with parametric uncertainties, Structural Safety 5 (3) (1988) 205–225.
[16] D.K. Kwon, T. Kijewski-Correa, A. Kareem, E-analysis of high-rise buildings subjected to wind loads, Journal of Structural Engineering 134 (7) (2008) 1139–1153.
[17] K.M. Lam, A. Li, Mode shape correction for wind-induced dynamic responses of tall buildings using time-domain computation and wind tunnel tests, Journal of Sound and Vibration 322 (4–5) (2009) 740–755.
[18] MATLAB, User Guide. The MathWorks, Inc., 2006
[19] L. Rosa, G. Tomasini, A. Zasso, A.M. Aly, Wind-induced dynamics and loads in a prismatic slender building: modal approach based on unsteady pressure measures, Journal of Wind Engineering and Industrial Aerodynamics 107–108 (2012) 118–130.
[20] E. Simiu, R.H. Scanlan, Wind Effects on Structures, John Wiley & Sons, Inc., New York, USA, 1996.
[21] E. Simiu, Wind loading codification in the Americas: fundamentals for a renewal, in: Proceedings of the 11th Americas Conference on Wind Engineering, San Juan, Puerto Rico, USA, June 2009.
[22] E. Simiu, R.D. Gabbai, W.P. Fritz, Wind-induced tall building response: a time-domain approach, Wind and Structures 11 (6) (2008) 427–440.
[23] K.T. Tse, P.A. Hitchcock, K.C.S. Kwok, Mode shape linearization for HFBB analysis of wind-excited complex tall buildings, Engineering Structures 31 (3) (2009) 675–685.
[24] J.R. Wu, Q.S. Li, A.Y. Tuan, Wind-induced lateral-torsional coupled responses of tall buildings, Wind and Structures 11 (2) (2008) 153–178.
[25] D. Yeo, E. Simiu, High-rise reinforced concrete structures: database-assisted design for wind, Journal of Structural Engineering 137 (11) (2011) 1340–1349.
[26] D. Yeo, E. Simiu, Database-assisted design for wind effects on high-rise structures and its potential for assessment of CFD simulation, in: Proceedings of the Fifth International Symposium on Computational Wind Engineering (CWE2010), Chapel Hill, North Carolina, USA, 2010.
[27] D. Yeo, Database-assisted design for high-rise structures in mixed extreme wind climates, in: Proceedings of the 13th International Conference on Wind Engineering ICWE-13, Amsterdam, July 11–15, 2011.
[28] D. Yeo, Simiu, Database-Assisted Design for Wind: Veering Effects on High-Rise Structures, Technical Note No. 1672, National Institute of Standards and Technology, Gaithersburg, MD, USA, June 2010b.
[29] A. Zasso, S. Giappino, S. Muggiasca, L. Rosa, Optimization of the Boundary Layer Characteristics Simulated at Politecnico di Milano Boundary Layer Wind Tunnel in a Wide Scale Ratio Ranger. The Sixth Asia-Pacific Conference on Wind Engineering, Seoul, Korea, 2005.
[30] A. Zasso, A.M. Aly, L. Rosa, G. Tomasini, Wind Induced Dynamics of a Prismatic Slender Building with 1:3 Rectangular Section, BBAA VI International Colloquium on Bluff Bodies Aerodynamics & Applications, Milano, Italy, 20–24 July, 2008.
[31] Y. Zhou, T. Kijewski, A. Kareem, Aerodynamic loads on tall buildings: interactive database, Journal of Structural Engineering 129 (3) (2003) 394–404.